Secondary hardening in laser rapidly solidified Fe-68(MoWCrVCoNiAlCu)(32) medium-entropy high-speed steel coatings

Materials and Design 159 (2018) 224–231

Contents lists available at ScienceDirect

Materials and Design

journal homepage: www.elsevier.com/locate/matdes

Secondary hardening in laser rapidly solidified $Fe_{68}(MoWCrVCoNiAlCu)_{32}$ medium-entropy high-speed steel coatings

Hui Zhang [a,b,*], Bang Dou [a], Hao Tang [a], Yizhu He [a], Sheng Guo [c]

[a] School of Materials Science and Engineering, Anhui University of Technology, Ma'anshan, 243002, Anhui, PR China
[b] State Key Laboratory of Solid Lubricating, Lanzhou Institute of Chemical Physics, Chinese Academic of Science, Lanzhou 730000, Gansu, PR China
[c] Department of Industrial and Materials Science, Chalmers University of Technology, SE-41296 Gothenburg, Sweden

HIGHLIGHTS

- New medium-entropy high speed steel coatings exhibit excellent hot wear resistance
- Secondary hardening due to coherent nano-sized M_2C contributes to the high hardness
- The secondary hardening is enhanced with the increasing C content
- The C content needs to be optimized for high hardness and good hot wear resistance

GRAPHICAL ABSTRACT

Microstructure and hardness variation of novel $Fe_{68}(MoWCrVCoNiAlCu)_{32}$ medium-entropy high-speed steel (ME-HSS) coatings with different C content: 0.65 wt%C (ME-HSS-065C), 0.85 wt%C(ME-HSS-085C) and 1.05 wt%C(ME-HSS-105C).

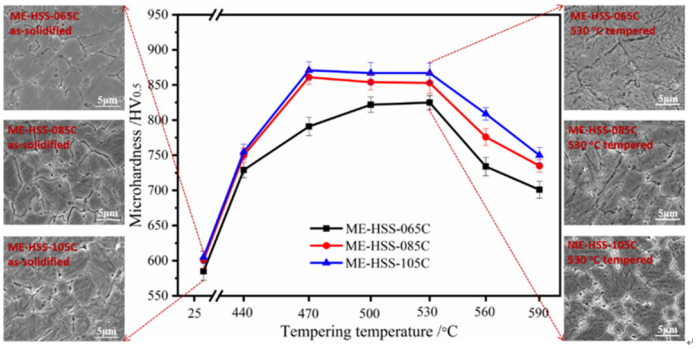

ARTICLE INFO

Article history:
Received 26 May 2018
Received in revised form 25 July 2018
Accepted 28 August 2018
Available online 31 August 2018

Keywords:
High speed steel
Coating
Medium-entropy alloy
Secondary hardening
Martensite

ABSTRACT

Novel $Fe_{68}(MoWCrVCoNiAlCu)_{32}$ (at.%) medium-entropy high-speed steel (ME-HSS) coatings, containing various carbon contents from 0.65 to 1.05 wt%, are prepared by laser rapid solidification. The newly prepared ME-HSS coatings are characterized by a hard martensitic matrix enhanced by secondary hardening, and specifically by coherent nano-sized M_2C. The secondary hardening effect is enhanced with the increasing carbon content. The high amount of alloying elements in ME-HSS coatings results in excellent oxidative wear resistance, without leading to serious compositional segregation and coarsening of carbides.

1. Introduction

High-entropy alloys (HEAs), which contain a high amount of alloying elements and tend to stabilize solid solutions due to the contribution from high configuration entropy, can exhibit strong solid solution strengthening, nano-precipitation hardening, excellent corrosion and oxidation resistance, and good thermal stability [1–5]. However, one challenge to HEAs for industrial applications is their high material cost, since most reported HEAs contain a high content of expensive elements like Co and Ni. Recently, the current authors revealed that the concept of Fe-rich medium-entropy alloy (MEAs), which

* Corresponding author.
E-mail address: huizhang@ahut.edu.cn (H. Zhang).

https://doi.org/10.1016/j.matdes.2018.08.050
0264-1275/

contains above 50 at.% of iron, can be quite effective to reduce the cost of HEAs, while still maintaining the entropic contribution to stabilize solid solutions over intermetallic compounds. Based on that, they designed the so-called medium-entropy stainless steels (MESS), which are comprised of simple bcc or fcc solid solution phases, and contain 50–65 at.% of Fe, above 13 at.% of Cr, and other 5 to 7 elements with similar atomic percentage [6]. MESS serve as a good example to showcase that the compositional space for the alloy design in traditional high alloy steels can be broadened, potentially with tailored phases, microstructure and properties.

In this work, a series of medium-entropy high-speed steels (ME-HSS) coatings containing various carbon contents are designed. The selection of alloying elements is based on the established knowledge for traditional HSS, which belong to complex Fe-C-X high alloy steels (X = Mo, W, Cr, V) containing a high carbon content, with the microstructure featuring a large volume of hard carbides, formed from eutectic reactions or secondary precipitation, distributing in a martensitic matrix [7,8]. It is already known that the selection and content of strong carbide-forming elements, like Cr, W, Mo and V, are critical in the carbide precipitation and hardness improvement of the HSS [9,10]. However, the traditional alloy design in HSS generally regards that a high amount of alloying elements would result in serious compositional segregation and fast growth of carbides, hence a low toughness of the steels.

Therefore, it is the purpose of this work to use the concept of MEAs to design new HSS with a high amount of alloying elements. There are three considerations that are taken into account when designing the alloy compositions and ways to prepare alloys. Firstly, the laser rapid solidification technique, which is one of the main non-equilibrium processing methods and can enhance solute trapping and relieve compositional segregation, is chosen to prepare ME-HSS. Previous studies have confirmed that laser cladded HSS coatings exhibit ultrafine microstructures, limited amount of precipitates and insignificant coarsening of carbides [11–13]. Secondly, apart from the carbide forming elements W, Mo, V and Cr, non-carbide forming elements Co, Al, Ni and Cu with the same content of 4at.% are also added to increase the number of alloying elements and hence the configuration entropy. Consequently, the calculated configuration entropy in the current HSS coating is about 1.29*R* (assuming in fully random solid solution states, and the carbon content is not counted. R is the gas constant). The current HSS can then be classified as MEAs, based on a widely accepted definition that defines MEAs as alloys having a configuration entropy between *R* and 1.5*R* [14]. Furthermore, it should be noted that the addition of non-carbide forming elements like Al and Co has been proved to benefit the improvement of thermal stability and oxidation resistance in traditional HSS [15,16]. Thirdly, the effect of various carbon contents, is studied in this work, aiming to obtain high hardening with carbide precipitation.

2. Experimental procedure

A series of $Fe_{68}(MoWCrVCoNiAlCu)_{32}$ (at.%) ME-HSS coatings containing various carbon contents, specifically 0.65 wt%, 0.85 wt% and 1.05 wt%, were prepared in this work. The three coatings with increasing carbon content are subsequently referred to as ME-HSS-065C, ME-HSS-085C and ME-HSS-105C, respectively. Powders used for ME-HSS coatings were mechanically mixed starting from pure metal powders. C was added into the mixed ME-HSS powders in the form of the ferrocarbide alloy (C: 4 wt%). The compositions of the ME-HSS alloys in weight percentage are as follows: 11.94 wt% W, 6.23 wt% Mo, 3.38 wt % Cr: 3.31 wt% V, 3.83 wt% Co, 3.81 wt% Ni, 4.13 wt% Cu, 1.75 wt% Al, 61.64 wt% Fe, with additional 0.65 wt%, 0.85 wt% and 1.05 wt% of C. All used powders were in the size range of 50–120 μm. For laser cladding, a 5 kW continuous-wave CO_2-laser system with directly focused laser beam was used. The mechanically mixed powders were preplaced onto the surface of a low carbon steel substrate to form a powder bed with a thickness of 1.0–1.5 mm. By the relative movement between the laser beam and the substrate, the preplaced powder was melted and a rapidly solidified single-track coating strongly bonded with the substrate was produced. The multi-tracks with a 30% overlap of each track were achieved by moving the laser beam back and forth. High-purity argon gas was used as the shielding gas through the coaxial nozzle to prevent oxidation. The laser power, beam diameter and scanning speed used here were 2.0 kW, 4.5 mm and 400 mm min^{-1}. After laser scanning, about 0.8 mm thick coatings together with a thin layer of melted substrate were obtained. Then the laser cladded coatings were tempered three times (triple-tempering) in the temperature range between 440 °C and 590 °C. Each tempering time was 60 min. The triple-tempering process is directly transferred from the routine heat treatment procedure for conventional HSS, and the purpose is to eliminate the influence from the possible existence of retained austenite [7,8].

The phase constitution and microstructure were characterized using a Rigaku X-ray diffractometer (XRD) with the Cu-Kα radiation, transmission electron microscopy (TEM) (Tecnai G2, 200 kV), and a Quanta 450 field emission gun scanning electron microscope (FEG-SEM) equipped with the energy dispersive spectrometer (EDS). SEM specimen was cut from the cross-section of the coatings, and the surface was etched using aqua regia before observation. TEM specimen was cut parallel to the substrate. The microhardness was measured at around the middle of the cross-section of the coatings, by a Vickers hardness tester with a load of 4.9 N and loading time of 30 s. Each alloy was tested for multiple points and the average hardness was calculated. Hot wear resistance was tested on a HT tribometer (MMU-100) with a pin-on-disc wear test device at 500 °C in ambient air. The diameter of contact surface of cylindrical pins was 4.0 mm. All samples were tested under a load of 50 N and a sliding velocity of 100 r/min for 115 min. After the hot wear test, the worn surface from both the coating, and the counterface made of the AISI M2 HSS, were observed by SEM. M2 is the "standard" and the most widely industry-used HSS with the composition W6Mo5Cr4V2 (in weight percentage) and a carbon content of 0.85 wt%.

3. Results

3.1. Hardness

Fig. 1 shows that the hardness variation in ME-HSS coatings after triple-tempering at different temperatures. All ME-HSS coatings show obvious secondary hardening, with the hardness increasing from about 585 HV, 601 HV and 615 HV, to the maximum value of 825 HV, 861 HV and 871 HV in the ME-HSS-065C, ME-HSS-085C and ME-HSS-105C coating, respectively. Apparently, a higher carbon content leads to a higher hardness and lower peak temperature for secondary hardening; secondary hardening peaks appear at 530 °C for ME-HSS-065C and at 470 °C for ME-HESS-085C and ME-HSS-105C. This observation indicates that the secondary hardening effect is enhanced with the increasing carbon content. When the triple-tempering temperature is above 530 °C, the hardness in all three ME-HSS coatings gradually decreases. The hardness variation seen in the ME-HSS coatings here is quite similar to that in the traditional Fe-C-X HSS [7,16,17]. Therefore, by analogy it can be inferred that secondary hardening in ME-HSS coatings should be caused by secondary carbide precipitation, while the decreased hardness after tempering at above 530 °C is due to carbide coarsening and tempering induced softening in the martensitic matrix, which will be proved by microstructural observations later. Darmawan et al. previously studied the laser cladded M2 coating, and they found that the maximum hardness in it is about 840 HV, after triple-tempering at 560 °C [13]. The maximum hardness after tempering in the current ME-HSS coatings is quite comparable with results obtained by Darmawan et al. in the M2 coating, indicating a high amount of alloying

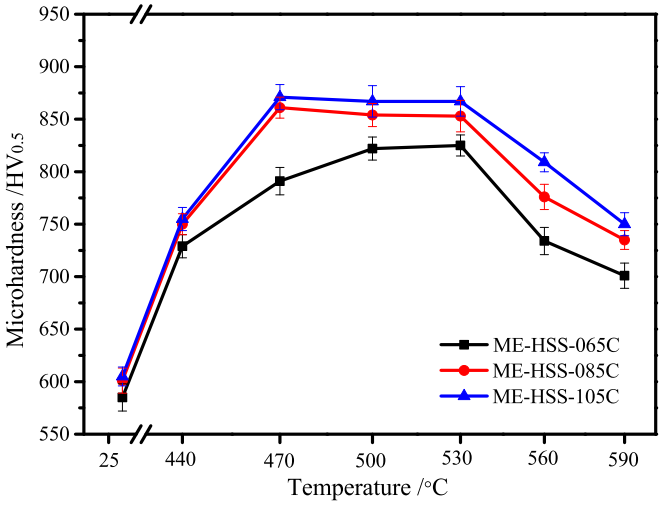

Fig. 1. Variation in hardness after triple-tempering at different temperatures.

elements does not necessarily lead to hardness improvement or reduction.

3.2. Phase identification and microstructure characterization

Fig. 2a and b show the XRD patterns of the ME-HSS coatings after solidification and triple-tempering at 530 °C, respectively. In the as-solidified state, all three coatings are mainly composed of the dominant bcc/bct phase, i.e., the martensite. The amount of carbide phases in low, seen from the diffraction peaks with low intensities at around 40° in the XRD pattern (Fig. 2a), suggesting that the growth of carbides can be effectively restricted owing to the limited short-range solute diffusion during the laser rapid solidification. After triple-tempering at 530 °C, M_2C carbide is noticeably detected in the ME-HSS-105C coating and also in ME-HSS-085C, which further proves that the increasing carbon content enhances the carbide precipitation in the ME-HSS coatings.

Fig. 3a to c show that the as-solidified microstructures of three ME-HSS coating are all featuring with a martensitic matrix and homogeneously distributed carbides along grain boundaries. The microstructure seen here in the ME-HSS is quite similar to what is seen in traditional HSS [18,19]. As can be seen, the fully-grown plate-martensite spanning across the whole grain are visible in Fig. 3b and c, but not in Fig. 3a. The plate martensite originating from the same area in the austenitic grain and intersecting with other plates suggests that the martensitic transformation in the ME-HSS-085C and ME-HSS-105C coatings is of the burst type. The size of the plate martensite is restricted to several micrometers, indicating a significant amount of undercooling has been achieved in the coatings during the laser rapid solidification. The matrix in the ME-HSS-065C coating should be classified as the cryptocrystalline martensite, which is verified by the lath martensite by TEM observation in the next section. Moreover, it is found that the increasing carbon content does not result in the fast growth of hard carbides in the ME-HSS-085C and ME-HSS-105C coatings, which is in agreement with the XRD results. The carbide content in all three ME-HSS coatings is low (low diffraction peak intensities), far less in comparison with that in the bulk M2 HSS prepared by the conventional casting method (which can be easily detected by XRD) [10,15–17]. Consequently, less formation of coarsened carbides would surely decrease the nucleation and propagation tendency of cracks, which generally take place at the carbide/matrix interface, and sometimes travel through the carbides.

In Fig. 3(d-f), it is shown that the increasing carbon content leads to more carbide precipitation in the ME-HSS coatings after triple-tempering at 530 °C, which is most obvious for the ME-HSS-105C coating. Table 1 compares the elemental distribution in the martensitic matrix and carbides (marked by M and C, respectively, in Fig. 3c and f) both

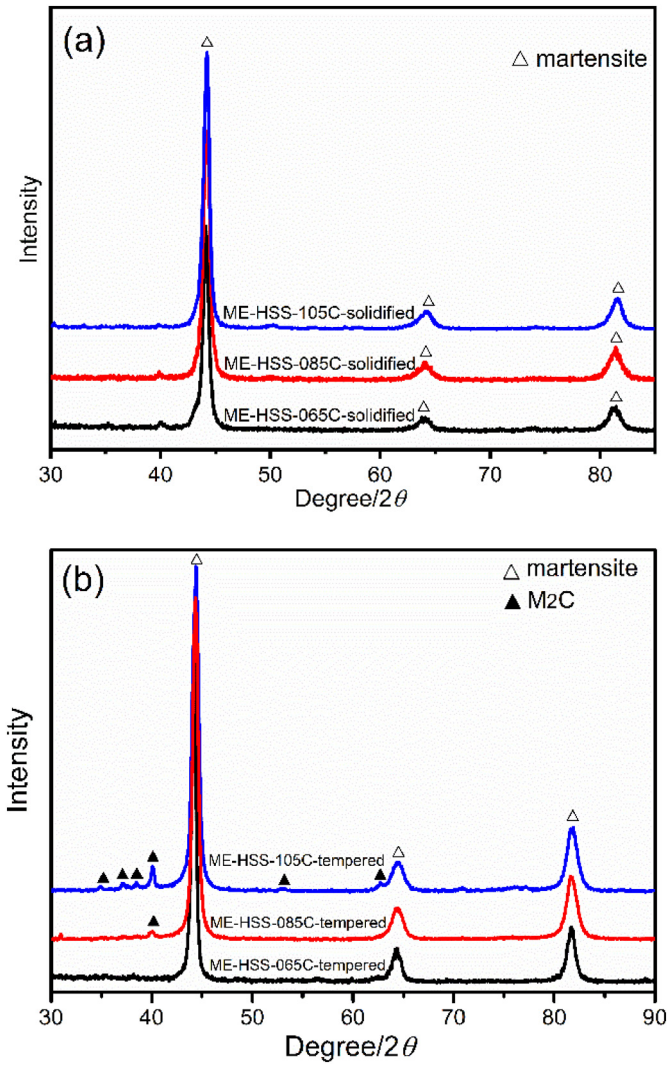

Fig. 2. XRD patterns of the ME coatings: (a) in solidified state; (b) after triple-tempering at 530 °C.

in the as-solidified and the tempered state of the ME-HSS-105C coating. As can be seen, non-carbide forming elements Ni, Co and Al are mainly distributed in the martensitic matrix, thus enhancing the solid solution strengthening in the supersaturated martensite. On the other hand, carbide-forming elements W, Mo, V and Cr are majorly enriched in carbides, and this can be seen more clearly and more convincingly from the EDS results, due to the growth of the carbides. In addition, it is noted that the Fe content in the martensitic matrix is much higher than the nominal Fe composition, which is possibly attributed to the dilution by the melted iron substrate, a common phenomenon seen in the laser cladding process [20,21].

3.3. TEM characterization

Fig. 4a confirms that the matrix in the as-solidified ME-HSS-065C coating comprises lath martensite, and a high density of dislocations. Fig. 4b shows the precipitated carbides at grain boundaries after triple-tempering at 530 °C. The corresponding selected area electron diffraction (SAED) pattern in Fig. 4c confirms the carbide is the hexagonal M_2C phase. The zone axis of the M_2C carbide is $[\bar{2}4\bar{2}3]$. The pyramidal plane of $(\bar{1}10\bar{2})$ meets the prism plane of $(\bar{1}010)$ at 70° and another pyramidal plane of $(01\bar{1}\bar{2})$ at about 40°. The ratio of inter-planar spacing between $(\bar{1}10\bar{2})$ and $(\bar{1}010)$ is 1.48. The lattice constants of *a* and *c* in

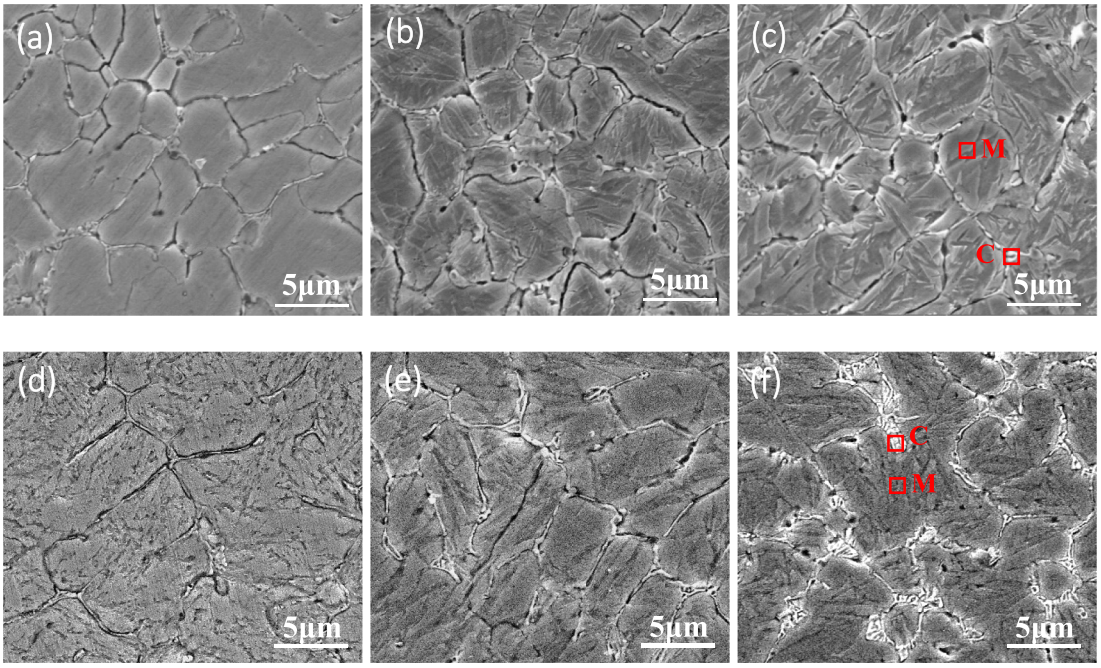

Fig. 3. Microstructure of ME-HSS-065C, ME-HSS-085C and ME-HSS-105C coatings, with the label C for carbides, and M for martensite: (a-c) in the as-solidified state; (d-f) after triple-tempering at 530 °C.

the hexagonal M_2C phase are measured to be 0.2923 nm and 0.4745 nm, respectively, which are slightly lower than 0.3011 nm and 0.4771 in the ideal Mo_2C crystal [22]. Previous studies have revealed that the c-axis lattice parameter of Mo_2C is sensitive to the carbon content, while the a-axis lattice parameter varies only weakly with the carbon content, but is more sensitive to the content of metallic alloying elements [23,24].

Fig. 5a and b present more details on the microstructure of the tempered ME-HSS-065C coating. It suggests that secondary hardening after triple-tempering at 530 °C originates mainly from the uniformly distributed nano-size carbides in the martensitic matrix, in addition to the solid solution strengthening in the supersaturated martensitic matrix. A similar scenario for secondary nano-precipitates has been widely seen in the early stage tempering of high carbon martensitic steels [25–27]. Uwakweh et al. claimed that the tweed-like modulated structure corresponds to two variants of carbon-rich and carbon-depleted regions formed during tempering [27]. Fig. 5c and d give the corresponding dark-field image and the SAED pattern for Fig. 5b. The dark-field image shows that the uniformly distributed nano-size carbides are of needle- or rod-like shape. Fig. 5d shows that the needle- or rod-shaped M_2C carbide has the coherent orientation relationship with the martensitic matrix (M): $(200)_M//(11\bar{2}0)M_2C$, $[013]_M//[11\bar{2}3]M_2C$.

Fig. 6 shows TEM images of the ME-HSS-105C coating after triple-tempering at 530 °C. The twined martensite can be clearly revealed by the midrib or the twin boundary, indicated by arrows, in Fig. 6a. Fig. 6b shows twinning in the plate martensite, and Fig. 6c and d further support the existence of micro-twins by the corresponding dark-field image and SAED pattern, respectively. Fig. 6e shows the tweed-like microstructure caused by uniformly distributed nano-size carbides, evidencing the existence of carbides in the coating.

3.4. Hot wear resistance

To obtain high performance in the HSS, including red hardness and hot wear resistance, many efforts have been made and much knowledge has been established. For example, it has been known that, apart from the carbide-forming elements Cr, W, Mo and V, Al can be used to enhance the homogeneous distribution of eutectic carbides and be beneficial for the high-temperature thermal stability of the traditional HSS [7,13–15]; Co can help to improve the red hardness of the martensitic matrix [16]. Meanwhile, a continuous and dense oxide film with good adhesion to the substrate is known to be able to reduce the friction coefficient and hence to improve the hot wear resistance [28,29]. Nevertheless, the content of anti-oxidation elements in the traditional HSS, such as M2, is generally low. Therefore, potentially the high alloying contents of Co, Ni, Al and Cr in the ME-HSS could result in a better performance for the ME-HSS coatings.

Fig. 7 presents the variation of friction coefficients with time, for the three ME-HSS coatings during the hot wear testing at 500 °C. Before testing, the coatings were firstly triple-tempered at 530 °C to obtain their maximum hardness or near-maximum hardness (refer to Fig. 1), and they were then heated toward 500 °C at a rate of 10 °C/min, and held at 500 °C for 10 min to let the oxidation film grow. It is seen that the ME-HSS-065C coating has a lower friction coefficient and hence a higher hot resistance than that in the ME-HSS-085C and ME-HSS-

Table 1
EDS results in various regions (refer to Fig. 3) in the ME-HSS-105C coating (at.%).

Component	Regions	Fe	W	Mo	Cr	V	Co	Ni	Al	Cu
Nominal	–	68	4	4	4	4	4	4	4	4
As-solidified state	M	72.97	2.85	2.51	3.54	2.44	4.21	4.01	4.29	3.18
	C	60.15	8.44	9.44	6.45	8.51	0.56	1.24	0.84	4.37
Tempered state	M	73.10	2.13	2.16	3.33	2.84	3.91	4.21	4.71	3.61
	C	45.25	15.66	16.93	7.15	11.18	0.24	0.86	0.19	2.54

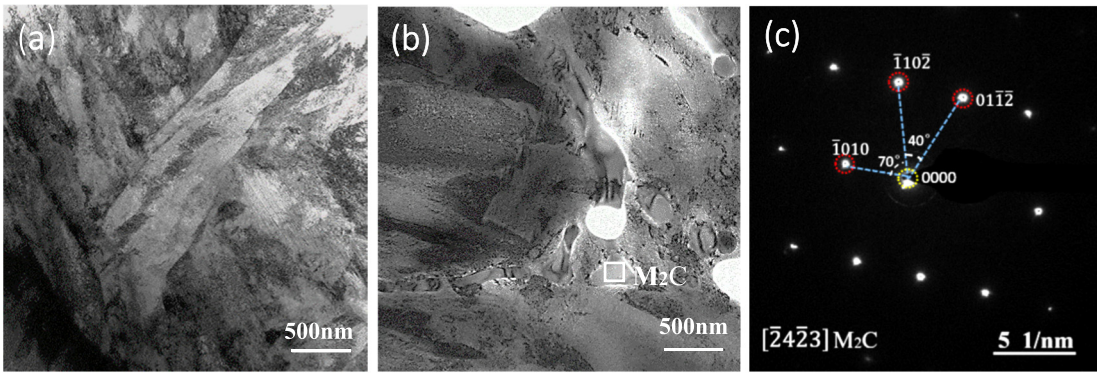

Fig. 4. TEM characterization of the ME-HSS-065C coating: (a) in the as-solidified state; (b) after-triple tempering at 530 °C; (c) the corresponding SAED pattern for the M2C carbide in (b).

105C coatings. Considering the maximum hardness after tempering (825 HV) is the lowest for ME-HSS-065C among three ME-HSS coatings, it is interesting to note here that a higher hardness is not always favorable for the better hot wear resistance. This interesting observation indicates that the carbon content, which is closely related to the hardness, should be set at an appropriate level to obtain high hardening for a better hot wear resistance in the laser cladded ME-HSS coatings. The reasoning behind is that the high content of precipitated carbides (at the grain boundaries) and the formation of plate martensite, both related to the high carbon content and contributing to the high hardness, can lead to embrittlement which has a negative effect on the hot wear resistance [19].

Fig. 8a and b compare the microstructure of worn surfaces, and local chemical compositions measured by EDS, on the ME-HSS-065C coating and the counterface made of M2 (with hardness of ~805 HV). EDS analysis shows that the oxygen content is about 30 wt% on the worn surface of the ME-HSS-065C coating (Fig. 8a), indicating a typical oxidative wear occurs, which prevents direct metal-to-metal contact. The sliding trace is smooth with some parallel shallow grooves along the direction of sliding. By comparison, many fine granular oxide particles are seen on the worn surface of the M2 counterface (Fig. 8b). The contrasting results here suggest that the formed oxide film on M2 is loose, while a continuous oxide film with good adhesion is formed on ME-HSS-065C and contributes to the good hot wear resistance in the latter. EDS results also confirm that Al and Cr are detected in the oxide film on the ME-HSS-065C coating, both elements known to be beneficial for the anti-oxidation. Fig. 8c and d show the worn surfaces of the ME-HSS-085C and ME-HSS-105C coatings, respectively. There exist no obvious oxide particles growing on the worn surface, indicating a good oxidation resistance of the two coatings. However, the smoothness and continuity (particularly the smoothness) of the oxide film are seen to decrease with the increasing carbon content, based on Fig. 8a, c and d. This observation again shows that the embrittlement caused by the high carbon content leads to a negative effect on the hot wear resistance.

4. Discussion

The microstructural characteristics, maximum tempering hardness and level of secondary hardening seen in ME-HSS coatings, with a high amount of alloying elements, are all quite similar to those in the

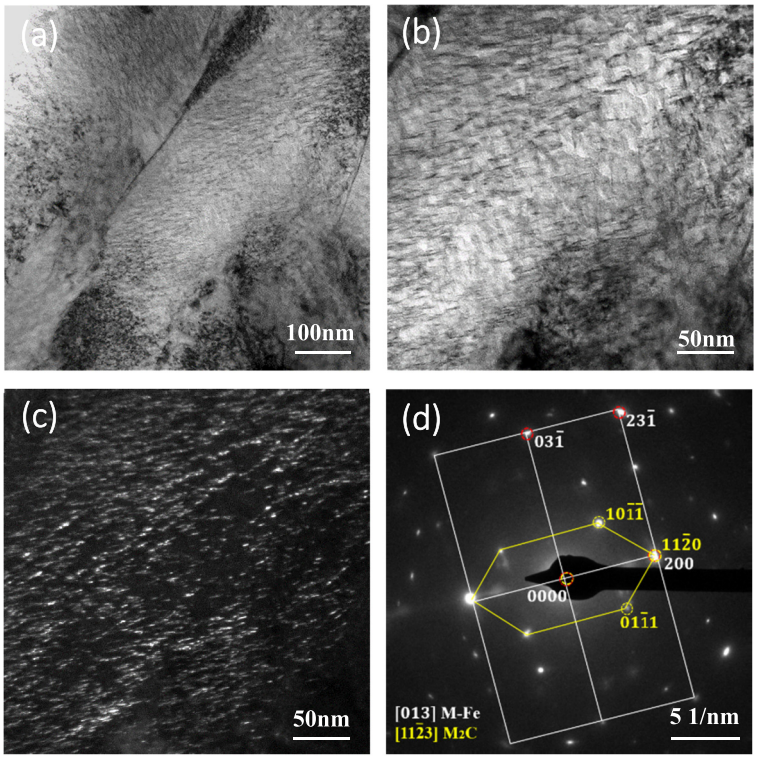

Fig. 5. TEM characterization of the ME-HSS-065C coatings after triple-tempering at 530 °C: (a-b) bright field images; (c) dark field image; (d) the corresponding SAED pattern for (b).

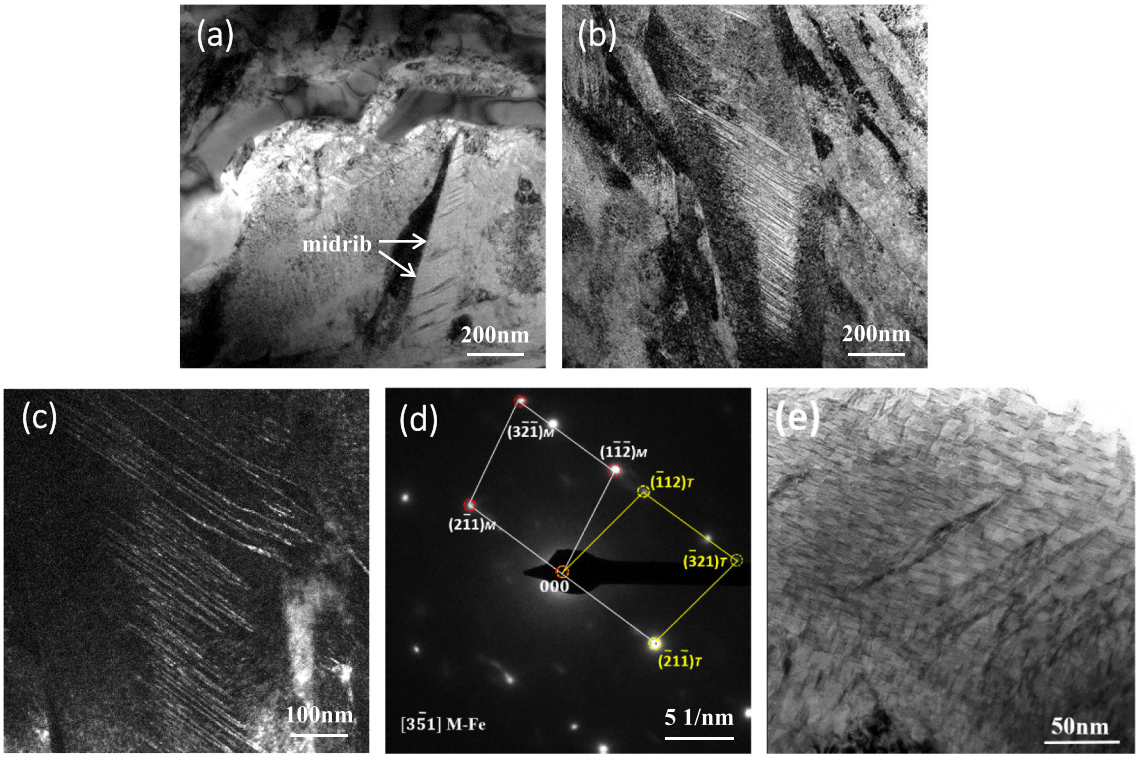

Fig. 6. TEM characterization of the ME-HSS-105C coating after triple-tempering at 530 °C: (a-b) bright field images; (c) dark field image of the twinned martensite; (d) the corresponding SAED pattern for (c); (e) tweed-like microstructure caused by secondary carbide precipitation.

traditional HSS coatings [8,12,13]. However, HE-MSS coatings can still be differentiated from traditional HSS coatings based on the following listed aspects.

Firstly, on the carbides. Park et al. concluded that the microstructural factors affecting the properties of HSS are (1) the type, morphology, volume fraction, and distribution of carbides; (2) the fine secondary carbides precipitated inside the matrix; and (3) the grain size of the solidified cell structure [30]. As for the type of carbides, it is already known that MC and M_2C are harder and regarded as better than the brittle fish-bone like M_6C or $M_{23}C_6$, among the complex carbides that could form in the HSS [10,31]. In the laser rapidly solidified ME-HSS coatings, the carbides are mainly M_2C as verified by XRD and TEM. Other brittle carbides may exist but their content should be very limited. The reason is attributed to the high content of Mo, Co, Ni, and Al, which are all believed to promote the formation of M_2C according to previous studies (instead, W favors the formation of M_6C and V favors the formation of MC) [32,33]. Furthermore, the secondary hardening could be enhanced with the high content of alloying elements, as the supersaturated solid solution is known to be thermodynamically unstable.

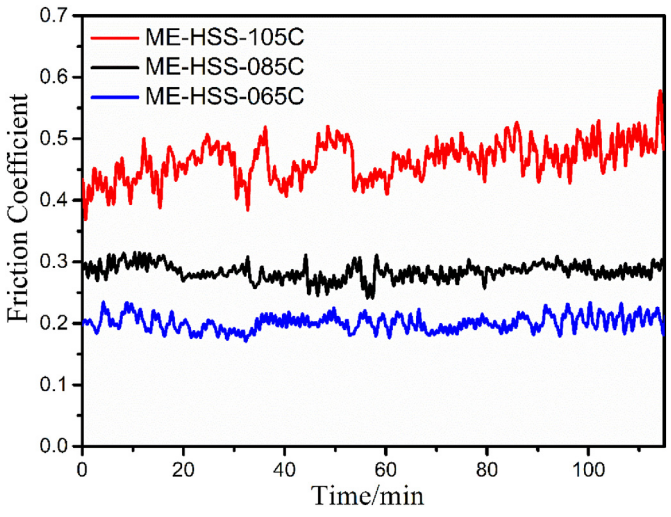

Fig. 7. The variation of friction coefficients with time for the ME-HSS coatings during the hot wearing test at 500 °C.

Secondly, on the retained austenite. Retained austenite is generally seen in the traditional HSS, but is not observed in the ME-HSS coatings. The reduced content of retained austenite is desirable as it is generally regarded as a harmful phase which can decrease the hardness of the HSS [10,34]. Several past studies actually showed that the laser rapid solidification tends to increase the content of retained austenite in the M2 coating [10,35,36]. Therefore, the less amount (not detectable by XRD) of retained austenite seen in the ME-HSS coatings, could be only related to the alloying elements, rather to the rapid solidification. Indeed, some elements like Co and Al are known to be effective in increasing the martensite finish (M_f) temperature in carbon steels [37].

Thirdly, on the morphology of martensite and ease of twinning. From Fig. 3, it is known that the increasing carbon content renders the morphology of martensite to change from cryptocrystalline (lath martensite) to plate, from the ME-HSS-065C coating to the ME-HSS-105C coating. The change to plate morphology is a typical feature for high carbon martensitic steels. Also, the formation of twinned martensite, as seen in Fig. 6, is often related to the low stacking fault energy (SFE) [38,39]. It therefore indicates that the newly designed ME-HSS alloys possess low SFE.

It is expected that the performance of the newly designed ME-HSS coatings can be further improved through tailoring and optimization of the alloy compositions, although the role of individual alloying elements still needs to be further studied in the future.

5. Conclusions

(1) A series of laser rapidly solidifed novel $Fe_{68}(MoWCrVCoNiAlCu)_{32}$ ME-HSS coatings, with various carbon contents from 0.65 to

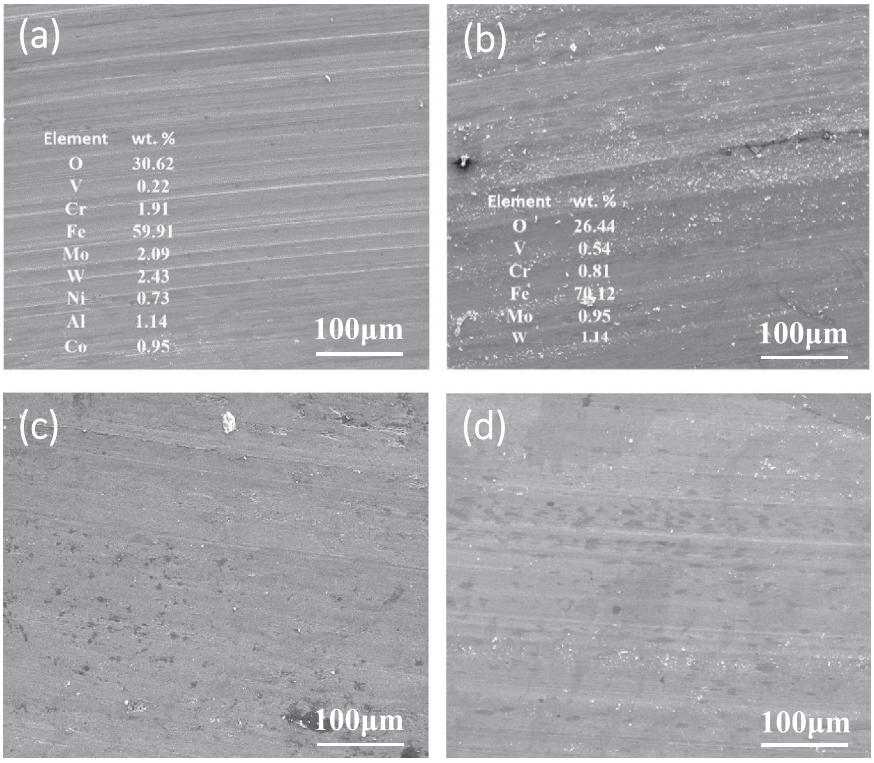

Fig. 8. Microstructure of worn surface after the hot wearing test. (a) the ME-HSS-065C coating (b) the counterface made of M2; (c) the ME-HSS-085C coating; (d) the ME-HSS-105C coating.

1.05 wt%, are designed and prepared in this work. These ME-HSS coatings comprise mainly a hard martensitic matrix, and exhibit strong secondary hardening that is attributed to the precipitation of nano-size M_2C after tempering.

(2) The newly designed ME-HSS coatings with a high amount of alloying elements do not present serious compositional segregation and coarsened carbides, and they possess excellent hot wear resistance.

(3) The carbon content in the ME-HSS is suggested to be controlled to obtain cryptocrystalline or lath martensite, rather than plate martensite, for the better hot wear resistance.

Acknowledgements

The authors thank the financial support from Joint Fund of Iron and Steel Research by National Natural Science Foundation of China (NSFC) under Grant No. U1560105 and the Open Fund from State Key Laboratory of Solid Lubricating under Grant No. LSL-1714. Yizhu He thanks for the financial support from NSFC under Grant No. 51271001.

References

[1] B. Gludovatz, A. Hohenwarter, D. Catoor, E.H. Chang, E.P. George, R.O. Ritchie, A fracture-resistant high-entropy alloy for cryogenic applications, Science 345 (2014) 1153–1158.
[2] J.W. Yeh, S.K. Chen, S.J. Lin, J.Y. Gan, T.S. Chin, T.T. Shun, C.H. Tsau, S.Y. Chang, Nanostructured high-entropy alloys with multiple principal elements: novel alloy design concepts and outcomes, Adv. Eng. Mater. 6 (2004) 299–303.
[3] J.Y. He, H. Wang, H.L. Huang, X.D. Xu, M.W. Chen, Y. Wu, X.J. Liu, T.G. Nieh, Z.P. Lu, A precipitation-hardened high-entropy alloy with outstanding tensile properties, Acta Mater. 102 (2016) 187–196.
[4] Y.L. Zhao, T. Yang, J. Wang, J.H. Luan, Z.B. Jiao, D. Chen, Y. Yang, A. Hu, C.T. Liu, J.J. Kai, Heterogeneous precipitation behavior and stacking-fault-mediated deformation in a CoCrNi-based medium-entropy alloy, Acta Mater. 138 (2017) 72–82.
[5] H. Zhang, Y. Pan, Y.Z. He, Synthesis and characterization of FeCoNiCrCu high-entropy alloy coating by laser cladding, Mater. Des. 32 (2011) 1910–1915.
[6] H. Zhang, H. Tang, W.H. Li, J.L. Wu, X.C. Zhong, Novel high-entropy and medium-entropy stainless steels with enhanced mechanical and anti-corrosion properties, Mater. Sci. Technol. 34 (2017) 1–8.
[7] S. Ma, W. Pan, J. Xing, S. Guo, H. Fu, Microstructure and hardening behavior of Al-modified Fe-1.5 wt%B-0.4 wt%C high-speed steel during heat treatment, Mater. Charact. 132 (2017) 1–9.
[8] N. Hashemi, A. Mertens, H.M. Montrieux, J.T. Tchuindjang, O. Dedry, Oxidative wear behaviour of laser clad high speed steel thick deposits: influence of sliding speed, carbide type and morphology, Surf. Coat. Technol. 315 (2017) 519–529.
[9] L.J. Xu, X.M. Fan, S.Z. Wei, D.D. Liu, H. Zhou, G.S. Zhang, Y.C. Zhou, Microstructure and wear properties of high-speed steel with high molybdenum content under rolling-sliding wear, Tribol. Int. 116 (2017) 39–46.
[10] M. Boccalini, H. Goldenstein, Solidification of high speed steels, Int. Mater. Rev. 46 (2) (2001) 92–115.
[11] G.F. Sun, K. Wang, R. Zhou, A.X. Feng, W. Zhang, Effect of different heat-treatment temperatures on the laser cladded M3:2 high-speed steel, Mater. Des. 65 (2015) 606–616.
[12] H.J. Niu, I.T.H. Chang, Microstructural evolution during laser cladding of M2 high-speed steel, Metall. Mater. Trans. A 31 (2000) 2615–2625.
[13] W. Darmawan, J. Quesada, F. Rossi, R. Marchal, F. Machi, Improvement in wear characteristics of the AISI M2 by laser cladding and melting, J. Laser Appl. 21 (2009) 176–182.
[14] D. Raabe, C.C. Tasan, H. Springer, M. Bausch, From high-entropy alloys to high-entropy steels, Steel Res. Int. 86 (2015) 1127–1138.
[15] X.X. Zhou, F. Fang, Y.Y. Tu, J.Q. Jiang, H.X. Xu, W.L. Wang, Effect of aluminum on the solidification microstructure of M2 high speed steel, Acta Metall. Sin. 50 (2014) 769–776.
[16] H.K. Moon, K.B. Lee, H. Kwon, Influences of Co addition and austenitizing temperature on secondary hardening and impact fracture behavior in P/M high speed steels of W–Mo–Cr–V(–Co) system, Mater. Sci. Eng. A 474 (2008) 328–334.
[17] S. Sackl, H. Leitner, H. Clemens, S. Primig, On the evolution of secondary hardening carbides during continuous versus isothermal heat treatment of high speed steel HS 6-5-2, Mater. Charact. 120 (2016) 323–330.
[18] H. Wang, L. Hou, J. Zhang, L. Lu, H. Cui, The secondary precipitates of niobium-alloyed M3:2 high speed steel prepared by spray deposition, Mater. Charact. 106 (2015) 245–254.
[19] R. Wang, G.L. Dunlop, The crystallography of secondary carbide precipitation in high speed steel, Acta Metall. 32 (1984) 1591–1599.
[20] Y. Cai, Y. Chen, S.M. Manladan, Z. Luo, F. Gao, Influence of dilution rate on the microstructure and properties of FeCrCoNi high-entropy alloy coating, Mater. Des. 142 (2018) 124–137.
[21] C. Ni, Y. Shi, J. Liu, G.Z. Huang, Characterization of $Al_{0.5}FeCu_{0.7}NiCoCr$ high-entropy alloy coating on aluminum alloy by laser cladding, Opt. Laser Technol. 105 (2018) 257–263.
[22] L. Jiang, W.Z. Zhang, Z.F. Xu, H.F. Huang, X.X. Ye, B. Leng, L. Yan, Z.J. Li, T. Hou, M_2C and M_6C carbide precipitation in Ni-Mo-Cr based superalloys containing silicon, Mater. Des. 112 (2016) 300–308.

[23] C.A. Knepfler, K.T. Faber, J. Weertman, G.B. Olson, C.R. Hubbard, O.B. Cavin, N. Packen, High temperature stability and thermal expansion behavior of molybdenum-chromium M_2C carbides, J. Alloys Compd. 248 (1997) 139–142.
[24] E. Rudy, S. Windisch, A.J. Stosick, J.R. Hoffman, The constitution of binary molybdenum-carbon alloys, Trans. AIME 239 (1967) 1247–1267.
[25] K.S. Cho, J.H. Choi, H.S. Kang, S.H. Kim, K.B. Lee, H.R. Yang, H. Kwon, Influence of rolling temperature on the microstructure and mechanical properties of secondary hardening high Co–Ni steel bearing 0.28 wt% C, Mater. Sci. Eng. A 527 (2010) 7286–7293.
[26] O.N.C. Uwakweh, J.M.R. Génin, J.F. Silvain, Electron microscopy study of the aging and first stage of tempering of high-carbon Fe-C martensite, Metall. Trans. A. 22 (1991) 797–806.
[27] O.N.C. Uwakweh, J.M.R. Génin, Morphology and aging of the martensite induced by cathodic hydrogen charging of high-carbon austenitic steels, Metall. Trans. A. 22 (1991) 1979–1991.
[28] E.M.D. Nascimento, L.M.D. Amaral, A.S.C.M. D'Oliveira, Characterization and wear of oxides formed on CoCrMoSi alloy coatings, Surf. Coat. Technol. 332 (2017) 408–413.
[29] L.D. Conceição, A.S.C.M. D'Oliveira, The effect of oxidation on the tribolayer and sliding wear of a Co-based coating, Surf. Coat. Technol. 288 (2016) 69–78.
[30] J.W. Park, C.L. Huo, S. Lee, Composition, secondary microstructure, hardness, and wear properties of high-speed steel rolls, Metall. Mater. Trans. A 30 (1999) 399–409.
[31] L.J. Xu, S.Z. Wei, F.N. Xiao, H. Zhou, G.S. Zhang, Effects of carbides on abrasive wear properties and failure behaviours of high speed steels with different alloy element content, Wear (2017) 968–974.
[32] C.K. Kim, J.I. Park, S. Lee, Y.C. Kim, N.J. Kim, J.S. Yang, Effects of alloying elements on microstructure, hardness, wear resistace, and surface roughness of centrifugally cast high-speed steel rolls, Metall. Mater. Trans. A 36 (2005) 87–97.
[33] H. Halfa, M. Eissa, K.E. Fawakhry, T. Matta, Effect of nitrogen and niobium on the structure and secondary hardening of super hard high speed tool steel, Steel Res. Int. 83 (2012) 32–42.
[34] T.H. Yu, J.R. Yang, Effect of retained austenite on GPM A30 high-speed steel, J. Mater. Eng. Perform. 16 (2007) 500–507.
[35] K.Y. Benyounis, O.M. Fakron, J.H. Abboud, Rapid solidification of M2 high-speed steel by laser melting, Mater. Des. 30 (2009) 674–678.
[36] J.J. Candel, P. Franconetti, V. Amigo, Study of the solidification of M2 high speed steel laser cladding coatings, Rev. Metal. 49 (2013) 369–377.
[37] G.E. Totten, Steel Heat Treatment Handbook, CRC, Taylor & Francis, 1997.
[38] M.J. Carr, J.R. Strife, G.S. Ansell, An investigation of the effects of austenite strength and austenite stacking fault energy on the morphology of martensite in Fe-Ni-Cr-0.3C alloys, Metall. Trans. A. 9 (1978) 857–864.
[39] A.M. Condă, F.C. Lovey, V. Torra, Interaction of twin boundaries with stacking faults in 2H martensite: a high-resolution electron microscopy study, Philos. Mag. 83 (2003) 1479–1493.